Amorphous structure of the immiscible $Fe_{1-y}(Cu_{1-x}Ag_x)_y$ alloy system

1991 J. Phys.: Condens. Matter 3 9859

(http://iopscience.iop.org/0953-8984/3/49/003)

J. Phys.: Condens. Matter 3 (1991) 9859–9869. Printed in the UK

Amorphous structure of the immiscible $Fe_{1-y}(Cu_{1-x}Ag_x)_y$ alloy system

K Sumiyama†‡, K Nishi† and K Suzuki‡

† Department of Metal Science and Technology, Kyoto University, Kyoto 606, Japan

‡ Institute for Materials Research, Tohoku University, Sendai 980, Japan

Received 19 November 1990, in final form 3 April 1991

Abstract. $Fe_{1-y}(Cu_{1-x}Ag_x)_y$ alloys sputter deposited on liquid-nitrogen-cooled substrates have been investigated by x-ray diffraction and differential scanning calorimetry measurements. Although this ternary alloy system is of a typically immiscible type in the equilibrium state, a single BCC phase appears at the Fe-rich corner and a single FCC phase at the Cu- and Ag-rich corners, while an amorphous phase appears in the central concentration region. In the interference function of the ternary amorphous alloys, a broad first peak and splitting of the second and third peaks are detected, where the peak intensity is much weaker than those in the binary FCC alloys. The radial distribution function indicates that a tetrahedron is the dominant structure unit of the amorphous alloys, as expected from the dense random packing of hard or soft spheres. The stacking of tetrahedra is not sequential but the main coordination polyhedron is an icosahedron, because the average coordination number is 11–12.

1. Introduction

Non-equilibrium alloys have been produced by energizing and quenching procedures such as solid quenching, liquid quenching and vapour quenching (Turnbull 1981). During sputter deposition, which is a typical vapour-quenching method, a high-energy vapour solution is condensed onto a cold substrate, the surface diffusion of energized adatoms is restricted if the substrate is a good heat sink (Thornton 1977) and several random phases which are high-temperature phases have been realized (Sumiyama 1991). Fe forms no solid solution with Cu and Ag at room temperature, Fe and Ag are almost immiscible with each other even in the liquid state at 2300 K (Massalski *et al* 1986). A Cu–Ag alloy system is also of the two phase separation type and forms very narrow regions of the primary solid solutions (Massalski *et al* 1986). In binary Fe–Cu, Fe–Ag and Cu–Ag alloys produced by conventional RF diode sputtering; however, wide single-phase regions of BCC and FCC have been obtained (Sumiyama *et al* 1984, 1988, Kataoka *et al* 1985). Moreover, in ternary Fe–Cu–Ag alloys, which show very narrow ranges of liquid solutions in the Cu–Ag- and Fe–Cu-rich sides at high temperatures (Chang *et al* 1977), an amorphous phase has been successfully obtained by RF diode sputtering in the central concentration region together with the wide single phases of BCC at the Fe-rich corner and FCC at the Cu- and Ag-rich corners (Sumiyama *et al* 1988).

RF diode sputtering could not attain a sufficiently high deposition rate for producing bulk alloys and could not avoid plasma irradiation of the substrate. On the contrary, facing-target-type DC sputtering gives quite a high deposition rate and effectively reduces

0953-8984/91/499859 + 11 $03.50

Table 1. Sputtering parameters.

Background pressure	<80 μPa
Ar gas pressure	0.6 Pa
Magnetic field	5–12 kA m^{-1}
Substrate temperature	110 K
Input voltage	600 V
Input current	600 mA
Deposition rate	5 Å s^{-1}

plasma irradiation of the substrate, minimizing the substrate heating and Ar contamination (Naoe *et al* 1980), because two parallel targets are arranged facing their planes and the magnetic field is applied perpendicular to the target surfaces to enhance the magnetron motion of electrons for a high ionization rate of Ar atoms and to confine the plasma region in the space between the target planes.

In this study, we have produced bulk $Fe_{1-y}(Cu_{1-x}Ag_x)_y$ alloys by facing-target-type DC sputtering. We deal with the characteristic structure of these alloys through x-ray diffraction and differential scanning calorimetry (DSC) measurements.

2. Experimental procedure

Using facing-target-type DC sputtering equipment and composite targets with a stripe shape prepared from 99.9% pure Fe, Cu and Ag plates, we made alloy specimens of 10–30 μm thickness on liquid-nitrogen-cooled substrates. The alloy composition was adjusted by changing the surface ratio of Fe, Cu and Ag stripe plates. The sputtering conditions are indicated in table 1. The chemical compositions of sputter-deposited alloys were determined by an electron probe microanalysis (EPMA). The concentration distribution over the surface and the concentration difference between the free surface side and the substrate side were determined for some alloys, indicating a uniform concentration within an experimental error of about 2%.

X-ray diffraction patterns were observed at 290 K by using Fe Kα radiation or Mo Kα radiation. A graphite monochromator was used to eliminate the fluorescence x-ray and Kβ radiation from specimens. The x-ray intensity as a function of the scattering angle was measured stepwise in the two 2θ ranges, one from 10° to 30° and the other from 20° to 100°. The intensity of the small-angle part was smoothly connected to that of the large-angle part, and the interference function $Si(S)$ was obtained by normalization. The radial distribution function $G(r)$ was calculated from $Si(S)$ by

$$G(r) = 4\pi r^2\left(\sum_i c_i K_i\right)^2 g_0 + \frac{2r}{\pi}\left(\sum_i c_i K_i^2\right)\int_0^\infty Si(S)\sin(Sr)\,\mathrm{d}S \qquad (1)$$

and the reduced distribution function $g(r)$ by (Waseda 1980)

$$g(r) = G(r)\Big/4\pi r^2\left(\sum_i c_i K_i\right)^2 g_0. \qquad (2)$$

Here, c_i and K_i are the atomic concentration and the average electron number of the ith atom. The atomic density g_0 for the ternary $Fe_{1-y}(Cu_{1-x}Ag_x)_y$ alloys was estimated from

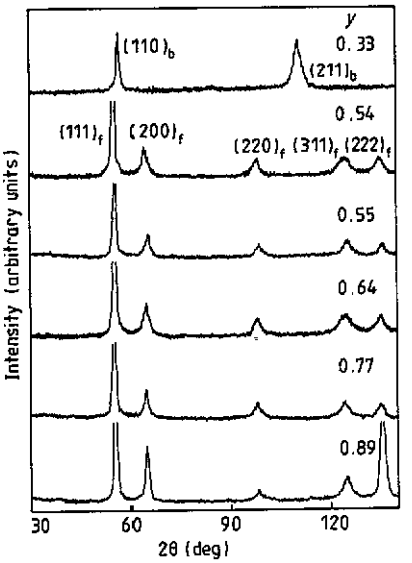

Figure 1. X-ray diffraction patterns for $Fe_{1-y}Cu_y$ alloys sputter deposited on liquid-nitrogen-cooled substrates.

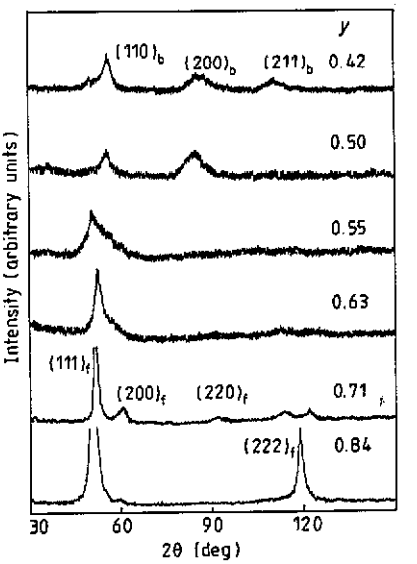

Figure 2. X-ray diffraction patterns for $Fe_{1-y}Ag_y$ alloys sputter deposited on liquid-nitrogen-cooled substrates.

the theoretical dependence of $G(r) = 0$ in the short-distance region in r, roughly agreeing with the values obtained by assuming the Vegard law between $Fe_{1-y}Cu_y$ and $Fe_{1-y}Ag_y$ alloys. DSC was done for deposited alloys in an Ar atmosphere with a heating rate of about 0.3 K s^{-1} in order to detect a sharp exothermic peak.

3. Experimental results

3.1. X-ray diffraction study by Fe Kα radiation

In the x-ray diffraction patterns for $Fe_{1-y}Cu_y$ alloys (figure 1), the BCC peaks are predominant for $y < 0.4$ and the FCC peaks for $y > 0.5$. In the x-ray diffraction patterns for $Fe_{1-y}Ag_y$ alloys (figure 2), the BCC peaks are predominant for $y < 0.5$ and the FCC peak for $y > 0.6$.

Figure 3 shows the x-ray diffraction patterns for $Fe_{1-y}(Cu_{1-x}Ag_x)_y$ alloys with $y \simeq 0.6$. The FCC peaks are observed for $x < 0.5$ and $x \simeq 1.0$, while a halo pattern indicating an amorphous structure is observed for $0.5 < x < 1.0$. In figure 4, the x-ray diffraction patterns for $Fe_{1-y}(Cu_{1-x}Ag_x)_y$ alloys with $x \simeq 0.5$ reveal the BCC peaks for $y < 0.55$ and the FCC peaks for $y > 0.65$, while a halo pattern for $0.55 < y < 0.65$ is found.

3.2. X-ray diffraction study by Mo Kα radiation

Figure 5 shows $Si(S)$ for $Fe_{1-y}(Cu_{1-x}Ag_x)_y$ alloys with $y \simeq 0.6$ as a function of the scattering vector $S = (4\pi \sin\theta)/\lambda$, where θ is the scattering angle and λ the x-ray wavelength. The sharp peaks are detected up to the high-S region for the binary FCC $Fe_{0.27}Cu_{0.73}$ and $Fe_{0.35}Ag_{0.65}$ alloys and the peak intensities are weaker in the latter alloy

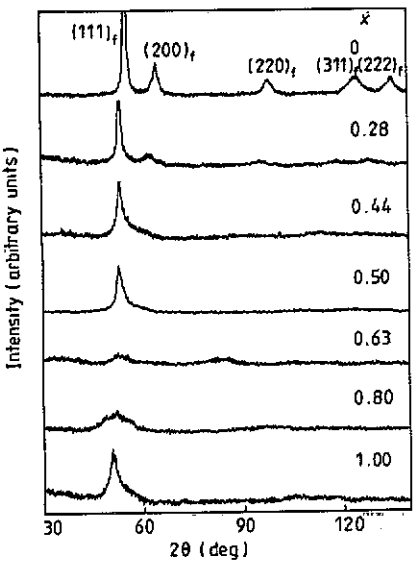

Figure 3. X-ray diffraction patterns for $Fe_{1-y}(Cu_{1-x}Ag_x)_y$ alloys with $y = 0.6$ sputter deposited on liquid-nitrogen-cooled substrates.

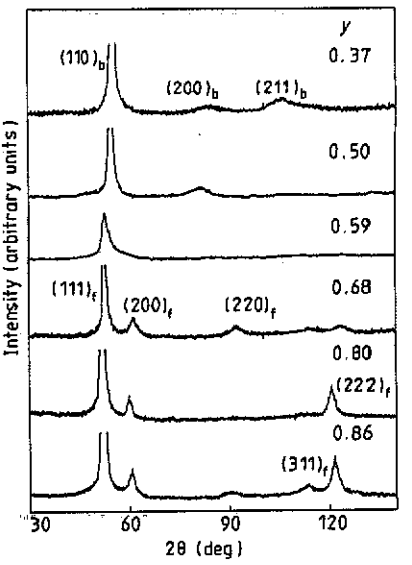

Figure 4. X-ray diffraction patterns for $Fe_{1-y}(Cu_{1-x}Ag_x)_y$ alloys with $x = 0.5$ sputter deposited on liquid-nitrogen-cooled substrates.

than in the former, partly owing to the high absorption probability of heavy Ag atoms. In the ternary amorphous alloys, a broad first peak and splitting of second and third peaks are detected, where the peak intensities are much weaker than those of the binary alloys and the oscillation of $Si(S)$ decreases rapidly for $S > 10$ Å^{-1}. The peak positions of $Si(S)$ shift to the low-S side with increase in the Ag concentration because the atomic radius of Ag is much larger than that of Cu (Darken and Gurry 1953).

Figures 6 and 7 show the radial distribution function $G(r)$ and the reduced radial distribution function $g(r)$ of $Fe_{1-y}(Cu_{1-x}Ag_x)_y$ alloys with $y \simeq 0.6$. Many clear peaks are detectable in the binary alloys and the peak width of the FCC $Fe_{0.35}Ag_{0.65}$ alloy is broader than that of the FCC $Fe_{0.27}Cu_{0.73}$ alloy, probably because the addition of Ag atoms with a large atomic radius introduces a much larger distribution in the near-neighbour distance. Three broad peaks are detected in the ternary $Fe_{0.42}(Cu_{0.52}Ag_{0.48})_{0.58}$ and $Fe_{0.37}(Cu_{0.46}Ag_{0.54})_{0.63}$ alloys at about 2.8, 4.7 and 7.2 Å. The broad first peak of $g(r)$ composed of nearest-neighbour atom pairs of Fe–Fe, Fe–Cu, Fe–Ag, Cu–Cu, Cu–Ag and Ag–Ag reveals no clear peak separation between the individual atom pairs, although the atomic radii of 1.26 Å for Fe, 1.27 Å for Cu and 1.47 Å for Ag are quite different (Darken and Gurry 1953). The first three peak positions shift with the change in x. However, the relative peak positions scaled to the first peak position of $g(r)$ are independent of the alloy concentration within the experimental error of ±0.03, as listed in table 2 and they correspond to the first, third and seventh peaks for the binary FCC alloys.

The average coordination number n_1, is estimated from the integrated intensity of the first peak of $G(r)$ in figure 6, provided that lack of chemical short-range order is assumed as is justified later in this paper. In table 2, $n_1 = 11$–12 where the n_1 value of the FCC $Fe_{0.27}Cu_{0.73}$ alloy is much smaller, probably because the large oscillation remaining in

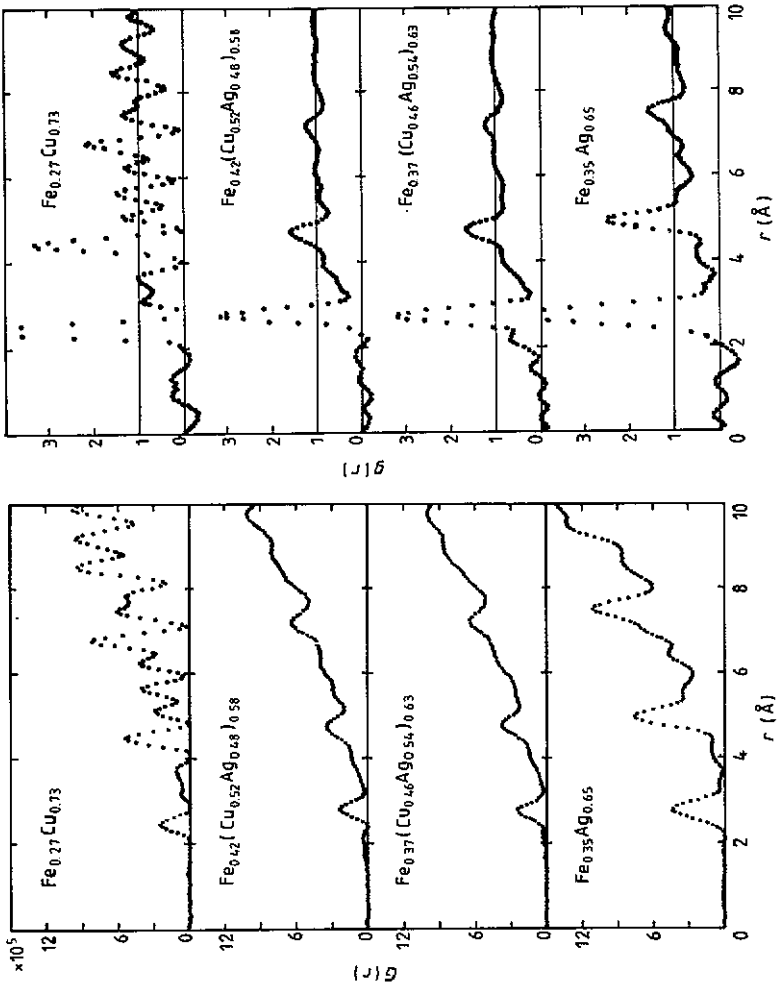

Figure 7. Reduced radial distribution function $g(r)$ of amorphous $Fe_{1-y}(Cu_{1-x}Ag_x)_y$ alloys with $y \simeq 0.6$ sputter deposited on liquid-nitrogen-cooled substrates.

Figure 6. Radial distribution function $G(r)$ of amorphous $Fe_{1-y}(Cu_{1-x}Ag_x)_y$ alloys with $y \simeq 0.6$ sputter deposited on liquid-nitrogen-cooled substrates.

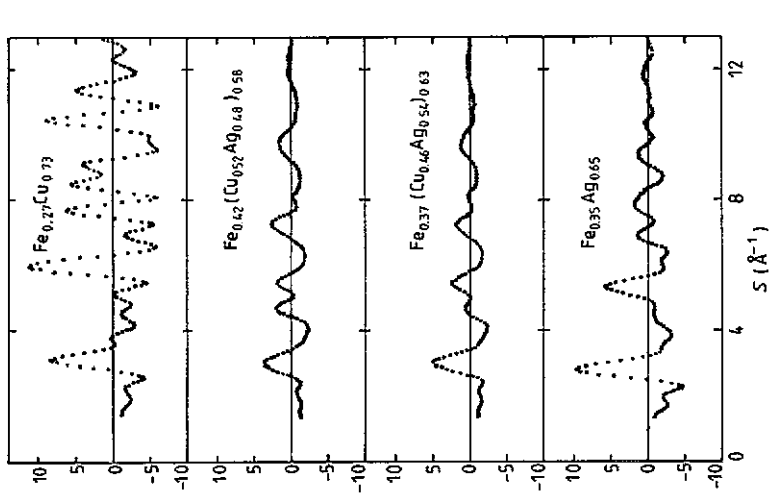

Figure 5. Interference function $Si(S)$ as a function of scattering vector S for amorphous $Fe_{1-y}(Cu_{1-x}Ag_x)_y$ alloys with $y \simeq 0.6$–0.7 sputter deposited on liquid-nitrogen-cooled substrates.

Table 2. Peak positions of $g(r)$ and coordination number n_1 for $Fe_{1-y}(Cu_{1-x}Ag_x)_y$ alloys sputter deposited on liquid-nitrogen-cooled substrates. The radial distance r_n, from the origin to the nth-neighbour atomic shell is indicated in the upper rows and the relative peak position r_n/r_1 scaled to the first peak position, in the lower rows.

y	x	r_1 Å r_1/r_1	r_2 Å r_2/r_1	r_3 Å r_3/r_1	r_4 Å r_4/r_1	r_5 Å r_5/r_1	r_6 Å r_6/r_1	r_7 Å r_7/r_1	r_8 Å r_8/r_1	n_1
0.73	0.0	2.45 1.0	3.67 1.50	4.45 1.82	5.13 2.09	5.63 2.30	6.25 2.55	6.75 2.76	—	9
0.58	0.48	2.78 1.0	—	4.70 1.69	—	—	—	7.19 2.59	—	11.2
0.63	0.54	2.75 1.0	—	4.74 1.72	—	—	—	7.22 2.63	—	11.1
0.65	1.0	2.76 1	—	4.95 1.79	5.57 2.02	6.42 2.33	7.00 2.54	7.50 2.72	—	12.5
FCC		1	1.41	1.73	2.0	2.24	2.45	2.65	2.83	12

the high-S range made the smoothing and normalization procedures ambiguous and gave a large error in the small-r range.

3.3. Differential scanning calorimetry

Since the halo pattern of the ternary $Fe_{1-y}(Cu_{1-x}Ag_x)_y$ alloys is rather sharp in comparison with other amorphous alloys, we checked whether a marked exothermic peak can be observed in the DSC trace of these alloys. Figure 8 shows the results for $Fe_{1-y}(Cu_{1-x}Ag_x)_y$ alloys with $y \simeq 0.6$, indicating that the alloys with $x = 0.5$–0.8 reveal a sharp exothermic peak. As shown in figure 9, $Fe_{1-y}(Cu_{1-x}Ag_x)_y$ alloys with $x \simeq 0.5$ also reveal a sharp exothermic peak for the alloys with $y \simeq 0.6$–0.8. The exothermic peak is ascribed to the crystallization of the amorphous phase and the crystallization temperature T_X was determined as the starting temperature of the exothermic effect. T_X is about 400 K and rather insensitive to the alloy concentration within the narrow single-phase region of the amorphous phase. These features are consistent with the results for the $Fe_{1-y}(Cu_{1-x}Ag_x)_y$ alloys produced by RF sputtering (Sumiyama *et al* 1988). The heat ΔQ of crystallization for amorphous alloys was estimated by integrating the sharp exothermic peak. As shown in table 3, the largest value of ΔQ is about 10 kJ mol^{-1} in the amorphous $Fe_{0.42}(Cu_{0.21}Ag_{0.79})_{0.58}$ alloy. On the other hand, non-equilibrium crystalline alloys decompose rather gradually to give no sharp exothermic peak. A rather broad exothermic peak above 500 K is probably due to the phase decomposition of non-equilibrium supersaturated alloys.

4. Discussion

Because of the preferred orientation of crystal growth and the large amount of strain in the present sputter-deposited specimens, we roughly estimated the ternary phase boundary diagram of $Fe_{1-y}(Cu_{1-x}Ag_x)_y$ alloys using the results of conventional x-ray

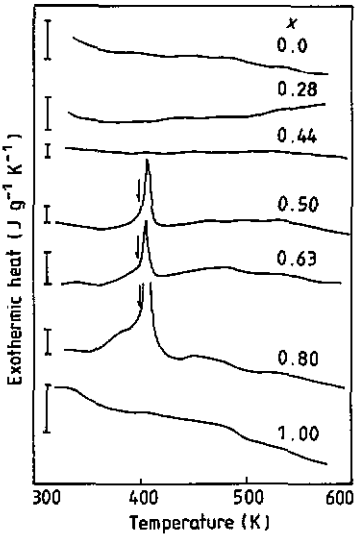

Figure 8. DSC traces obtained with a heating rate of 0.3 K s^{-1} for $Fe_{1-y}(Cu_{1-x}Ag_x)_y$ alloys with $y \simeq 0.6$ sputter deposited on liquid-nitrogen-cooled substrates. The vertical arrow indicates the crystallization temperature T_X.

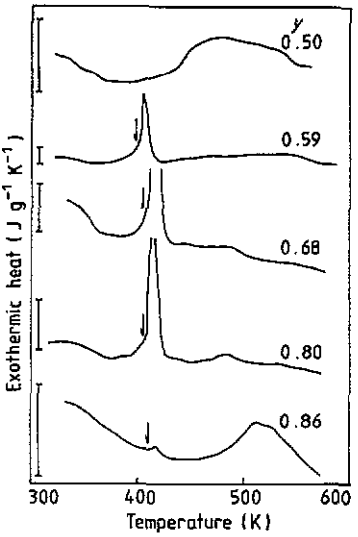

Figure 9. DSC traces obtained with a heating rate of 0.3 K s^{-1} for $Fe_{1-y}(Cu_{1-x}Ag_x)_y$ alloys with $x \simeq 0.5$ sputter deposited on liquid-nitrogen-cooled substrates. The vertical arrow indicates the crystallization temperature T_X.

Table 3. Heat, ΔQ of crystallization for sputter-deposited $Fe_{1-y}(Cu_{1-x}Ag_x)_y$ alloys.

y	x	ΔQ (kJ mol^{-1})	y	x	ΔQ (kJ mol^{-1})
0.58	0.0	—	0.55	0.0	—
0.58	0.28	—	0.55	1.0	—
0.60	0.44	—	0.50	0.55	—
0.59	0.50	2.6	0.68	0.46	3.2
0.60	0.63	1.3	0.80	0.51	2.6
0.58	0.80	10.3	0.86	0.46	0.1
0.63	1.0	—			

diffraction and DSC measurements. In figure 10, the single-phase region of BCC appears in the Fe-rich corner (rectangles) and that of FCC in the Cu- and Ag-rich corners (circles), while the single-phase region of the amorphous phase (triangles) displaying both a sharp exothermic peak in the DSC trace and a broad single peak in x-ray diffraction patterns is in the central concentration region. The full symbols indicate the alloys which display an exothermic peak in the DSC traces. This phase diagram is similar to that for $Fe_{1-y}(Cu_{1-x}Ag_x)_y$ alloys produced by RF sputtering (Sumiyama *et al* 1988). However, the single-phase regions of BCC and FCC phases are much wider and the region of the amorphous phase shifts to the higher-x side for $y \simeq 0.6$ in the present alloys compared with the previous alloys. The single-phase regions in the present ternary alloy diagram are wider than those in the previous diagram, suggesting that surface diffusion is much more suppressed and a mixed state of surface adatoms is more effectively quenched in

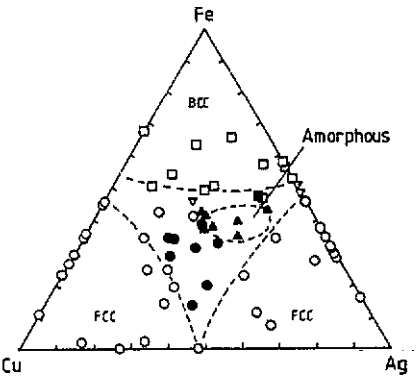

Figure 10. Non-equilibrium phase diagram of ternary $Fe_{1-y}(Cu_{1-x}Ag_x)_y$ alloys sputter deposited on liquid-nitrogen-cooled substrates. The results of x-ray diffraction measurements are shown as follows: □, the single BCC phase; ○, the single FCC phase; ▲, the single amorphous phase; ▽, the BCC and FCC mixed phase; ■, the BCC and amorphous mixed phase; ●, the FCC and amorphous mixed phase. The full symbols indicate the alloys which displayed an exothermic peak in the DSC trace.

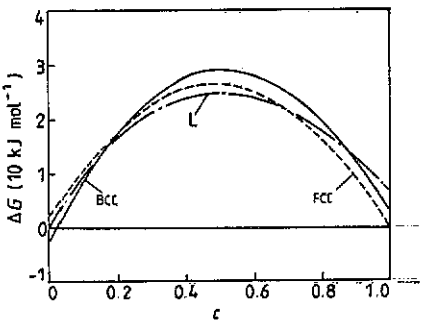

Figure 11. Free energy ΔG versus concentration c diagram at 500 K for $Fe_{1-c}Ag_c$ alloys (Swartzendruber 1984, Sumiyama 1991).

the deposition process of facing-target-type DC sputtering than in that of the previous RF sputtering.

The forming ability of non-equilibrium phases in diffusion-limited solid growth processes has been discussed by the free energy versus composition diagram (Massalski 1982). As shown in figure 11, for example, the ΔG–c diagram for $Fe_{1-c}Ag_c$ alloys predicts the formation of the BCC primary solid solution in the Fe-rich region and that of the FCC primary solid solution in the Ag-rich region (Swartzendruber 1984, Sumiyama 1991), in accordance with the experimental results (Kataoka *et al* 1985). The ΔG–c diagrams for $Fe_{1-c}Cu_c$ and $Cu_{1-c}Ag_c$ alloys also predict the wide concentration range of primary solid solutions in the vapour-deposited states, consistent with the experimental results (Sumiyama *et al* 1984, 1988). They also predict the formation of a supercooled liquid state, which can be regarded as an amorphous state, at the intermediate-concentration region of these binary alloys (see figure 11). However, we could obtain no binary amorphous alloys even on liquid-nitrogen-cooled substrates, although some reports indicated the formation of amorphous-like Fe–Ag and Cu–Ag alloys by vapour quenching (Chien and Unruh 1983, Reda *et al* 1982). In ternary $Fe_{1-y}(Cu_{1-x}Ag_x)_y$ alloys whose equilibrium phase diagram has not been reported in detail (Chang *et al* 1977), the amorphous phase is obtained at the central concentration region. This result suggests that the addition of the third element enhances the configurational entropy of deposited alloys and moderates the thermodynamical and/or kinetic conditions for amorphous phase formation.

As discussed in the previous paper (Sumiyama 1988), the empirical rules for the alloy phase formation, such as the size difference of constituent elements (Hume-Rothery

1966) and the mixing enthalpy ΔH_{mix} of equiatomic liquid alloys, or the formtion enthalpy ΔH_F of solid alloys (Güntherodt *et al* 1981, Simozar and Alonso 1984), reasonably explain the non-equilibrium BCC and FCC solid solutions in binary Fe–Cu, Fe–Ag and Cu–Ag alloys, but they do not explain the amorphous phase formation in the ternary $Fe_{1-y}(Cu_{1-x}Ag_x)_y$ alloys well. Indeed, the atomic size ratio of the constituent elements is larger than 10% for Fe–Ag and Cu–Ag and Fe–Cu–Ag alloys (Darken and Gurry 1953, Mader 1965); however, the amorphous phase is only formed in the ternary Fe–Cu–Ag alloys. Then, an amorphous phase is more favourable as ΔH_{mix} and ΔH_F are negative and their absolute values $|\Delta H_{mix}|$ and $|\Delta H_F|$ become larger. In particular, an amorphous phase is often formed in the rapidly quenched alloys with concentrations corresponding to the intermetallic compounds, in which ΔH_F is negative, $|\Delta H_F|$ is very large and the crystalline units are quite complicated and composed of a large number of atoms. In this context, the amorphous phase formation is unlikely for the ternary Fe–Cu–Ag alloys whose ΔH_{mix} and ΔH_F are positive (Sumiyama *et al* 1988, de Boer *et al* 1989).

The thermal stability of an amorphous phase strongly depends on the nucleation and growth kinetics of competing crystalline phases. However, on the assumption that the crystallization process of amorphous alloys is of a diffusion control type, its activation energy could be proportional to the formation enthalpy of a monovacancy having a size equal to that of a smaller or a larger atom, ΔH_{VS} or ΔH_{VL} (Buschow 1982, de Reus and Saris 1990). The crystallization temperature T_X is given by

$$T_X = C\,\Delta H_{VS} \qquad C = 7.5\ \text{K mol kJ}^{-1} \tag{3}$$

or

$$T_X = C'\,\Delta H_{VL} \qquad C' = 4.7\ \text{K mol kJ}^{-1}. \tag{4}$$

Since the atomic size of Fe is almost the same as that of Cu, we estimate ΔH_{VS} and ΔH_{VL} for pseudo-binary $(FeCu)_{0.5}Ag_{0.5}$ alloys to be about 96 kJ mol^{-1} and 118 kJ mol^{-1} (de Boer *et al* 1989), giving $T_X = 720$ K and 520 K. These T_X-values are much higher than the observed values.

As mentioned above, the amorphous phase formation is not well understood by the preceding empirical rules. However, the structure analysis gives a definite picture of the amorphous $Fe_{1-y}(Cu_{1-x}Ag_x)_y$ alloys. On comparison of the reduced radial distribution function $g(r)$ between the binary FCC and the ternary amorphous alloys, the peaks of the second- and fifth-neighbour positions disappear in the ternary amorphous alloys. These peaks are mainly ascribed to the half octahedral unit, while the third-, fourth-, sixth- and seventh-neighbour sites are ascribed to the tetrahedral unit in the FCC lattice (Suzuki 1990). The topological structures of amorphous metals and alloys are approximately described in terms of the dense random packing of hard spheres (DRPHS) model or the dense random packing of soft spheres (DRPSS) model (Bernal 1964, Finney and Wallace 1981), which are largely constructed from tetrahedral structure units, while in the FCC or BCC crystalline lattice both the tetrahedral and the octahedral structure units are included with a ratio of two to one. Therefore, the present results are consistent with these arguments; the octahedral structure units are disallowed and the tetrahedral units are preferentially formed during the sputter deposition process of ternary $Fe_{1-y}(Cu_{1-x}Ag_x)_y$ alloys.

The radial distribution function of amorphous metals and alloys has been interpreted by a spiral polytetrahedral cluster model shown in figure 12 (Takeuchi and Kobayashi 1981, Yasuda *et al* 1990); the amorphous structure is constructed by the sequential

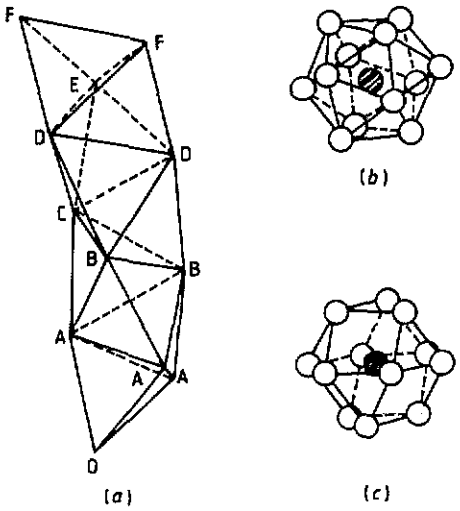

Figure 12. (*a*) Spiral polytetrahedral cluster model (Takeuchi and Kobayashi 1981), where the average radial distances are as follows: $\overline{OA} = 1$, $\overline{OB} = 1.65$, $\overline{OC} = 1.99$, $\overline{OD} = 2.49$, $\overline{OE} = 2.97$ and $\overline{OF} = 3.38$. (*b*) The icosahedral coordination unit. (*c*) The FCC coordination unit.

stacking of tetrahedra. Within this model the relative peak positions of atoms A, B, C, D, E and F scaled by the first peak for A atom are 1, 1.65, 1.99, 2.49, 2.97 and 3.38. Provided that the first peak of the ternary amorphous $Fe_{1-y}(Cu_{1-x}Ag_x)_y$ alloys in figures 6 and 7 is allotted to the position of atom A, the second peak can be allotted to the positions of atoms B and C and the third peak to the positions of atoms D and E. These results suggest that the stacking is not so sequential as displayed in figure 12(*a*). However, the average coordination number of 11–12 implies the close packing of Fe, Cu and Ag atoms in the present amorphous alloys. Since the DRPHS and DRPSS models indicate that the dominant coordination polyhedron is an icosahedron (figure 12(*b*)) composed of the tetrahedron (Bernal 1964, Briant and Burton 1978, Finney and Wallace 1981), the first-nearest-neighbour atomic correlation is supremely illuminating in the ternary amorphous Fe–Cu–Ag alloys.

The chemical short-range order is not taken into account in the present analysis. Since the Fe–Cu–Ag alloy system is of the typical immiscible type, chemical affinities between hetero-atom pairs do not surpass those between homo-atom pairs. In such an alloy system, the repulsive part of interatomic potential, i.e. the hard or soft core of constituent atoms, is dominant. Therefore, the ternary amorphous $Fe_{1-y}(Cu_{1-x}Ag_x)_y$ alloys are high-entropy metastable states consisting of topologically random packing of Fe, Cu and Ag atoms.

Acknowledgments

The authors wish to thank Professor Y Nakamura, Professor M Shiga, Dr H Yasuda, Mr Y Yokoyama and Mr R Iehara for their experimental support and encouragement, Professor P H Shingu for supporting the DSC measurements and Mr T Unesaki for doing the EPMA. They are also indebted to Mr S Kambara of Nihon Kogyo Ltd for preparing the Cu and Ag targets. This work was supported partially by a Grant-in-Aid for General Scientific Research (grant 01550507) given by the Ministry of Education, Science and Culture.

References

Bernal J D 1964 *Proc. R. Soc.* A **280** 299–322

Briant C L and Burton J J 1978 *Phys. Status Solidi* b **85** 393–402

Buschow K H J 1982 *Solid State Commun.* **43** 171–4

Chang Y A, Goldberg D and Neumann J P 1977 *J. Phys. Chem. Ref. Data* **6** 621–73

Chien C L and Unruh K M 1983 *Phys. Rev.* B **28** 1214–8

Darken L S and Gurry R W 1953 *Physical Chemistry of Metals* (New York: McGraw-Hill) pp 50–6

de Boer F R, Boom R, Mattens W C M, Miedema A R and Niessen A K 1989 *Cohesion in Metals* (Amsterdam: North-Holland) pp 219–58

de Reus R and Saris F W 1990 *Mater. Lett.* **9** 487–93

Finney J L and Wallace J 1981 *J. Non-Cryst. Solids* **43** 165–87

Güntherodt H J, Oelhafen P, Hauser E, Greuter F, Lapka R, Rösel F, Jacobs R, d'Albuquerque e Castro J, Kübler J, Hague C F, Bennemann K H, Fairlie R H, Temmermann W M and Gyorffy B L 1981 *Physics of Transition Metals 1980 (Inst. Phys. Conf. Ser. 55)* ed P Rhodes (Bristol: Institute of Physics) pp 619–29

Hume-Rothery W 1966 *The Structure of Alloys of Iron* (Oxford: Pergamon) ch 5

Kataoka N, Sumiyama K and Nakamura Y 1985 *J. Phys. F: Met. Phys.* **15** 1405–11

Mader S 1965 *J. Vac. Sci. Technol.* **2** 35–41

Massalski T B 1982 *Proc. Int. Conf. on Rapidly Quenched Metals* (Sendai: Japan Institute of Metals) pp 203–8

Massalski T B, Murray J L, Bennett L H and Baker H 1986 *Binary Alloy Phase Diagram* (Metals Park, OH: American Society for Metals)

Naoe M, Yamanaka S and Hoshi Y 1980 *IEEE Trans. Magn.* **MAG-16** 646–8

Reda I M, Hafner J, Pongratz P, Wagendristel A, Bangert H, Bhat P K 1982 *Phys. Status Solidi* a **72** 313–24

Simozar S and Alonso J A 1984 *Phys. Status Solidi* a **81** 55–61

Sumiyama K 1991 *Phys. Status Solidi* a **126** 1–22

Sumiyama K, Kawawake Y and Nakamura Y 1988 *Trans. Japan Inst. Met.* **29** 191–7

Sumiyama K, Yoshitake T and Nakamura Y 1984 *J. Phys. Soc. Japan* **53** 3160–5

Suzuki K 1990 *J. Non-Cryst. Solids* **117–8** 1–9

Swartzendruber L J 1984 *Bull. Alloy Phase Diagrams* **5** 560–4

Takeuchi S and Kobayashi S 1981 *Phys. Status Solidi* a **65** 315–20

Thornton J A 1977 *Annu. Rev. Mater. Sci.* **7** 239–60

Turnbull D 1981 *Metall. Trans.* A **12** 695–708

Waseda Y 1980 *The Structure of Non-Crystalline Materials* (New York: McGraw-Hill) ch 1

Yasuda H, Sumiyama K and Nakamura Y 1990 *J. Phys.: Condens. Matter* **2** 9967–74